Materials Research, Vol. 10, No. 4, 437-447, 2007

Using the Ratio: Maximum Load over Unload Stiffness Squared, P_m/S_u^2, on the Evaluation of Machine Stiffness and Area Function of Blunt Indenters on Depth-sensing Indentation Equipment

Juan Manuel Meza[a]*, *María Cristina Moré Farias*[b], *Roberto Martinz de Souza*[b], *Luis Javier Cruz Riaño*[c]

[a]*New Materials Research Group, Pontifical Bolivarian University, Circular 1 No 70-01, Medellín, Antioquia, Colombia*
[b]*Surface Phenomena Laboratory, Department of Mechanical Engineering, Polytechnic School, University of São Paulo – USP, Av. Prof. Mello Moraes, 2231, 05508-900 São Paulo - SP, Brazil*

Received: May 21, 2007; Revised: October 9, 2007

Depth sensing indentation study was conducted in a Fischerscope H100V machine, equipped with a Vickers indenter with a tip roundness of approximately 1330 nm. Tests were carried out on soda-lime glass, fused silica, sapphire, aluminum (1100 alloy), high alloyed steel, titanium and copper. The widely used iterative method of Oliver and Pharr was unsuccessful in the attempts to analyze machine compliance and indenter area function. Therefore, an alternative procedure was adopted. The alternative procedure is based on the ratio between maximum load and unload stiffness squared, P_m/S_u^2. It was found that this procedure, which is not iterative, gives good results. A careful study of the P_m/S_u^2 ratio, lead us to conclude that the Fischercope machine has a low compliance which depends on the sample mounting. This low compliance in conjunction with the recent discovery of the dependence of β factor on the tip roundness/maximum depth ratio, which appears in the relation between contact stiffness and contact area, explains why the iterative method does not converge. However, variations in β and machine compliance produces deviation on the hardness and elastic modulus lower that 6% with respect to expected values for the materials and the machine studied in this work.

Keywords: *depth-sensing indentation, nanoindentation, mechanical properties, machine compliance, tip roundness*

1. Introduction

The depth-sensing indentation technique has turned into one of the most important tools for the evaluation of the mechanical properties of coatings and bulk materials. The contact area is a paramount parameter required to analyze indentation data, since it is used for estimating elastic modulus, hardness and other material properties. Machine compliance, initial contact depth, thermal drift and indenter geometry should be taken into account, such that the contact area can be correctly estimated[1].

Currently, different methods are available[1-7] for the correction of tip bluntness, for Vickers and other types of indenters. The most accurate method is the topographic characterization by atomic force microscopy[5,7]; however, it is time consuming and requires large investments in terms of equipments and optical-laser sensors. The iterative method proposed by Oliver and Pharr[3] is widely used to obtain both the indenter geometry (area function) and machine compliance; however, the method is very sensitive to mathematical data treatment and, in some cases, it is not able to provide an accurate value of the area function[4,6,8,9]. The computational routines developed through the iterative method may lead to inaccurate results, due to an underestimation of the machine compliance[9]. In fact the iterative method does not converge for the Fischercope machine-tip used in this work. For this reason, a combination of the Doerner and Nix, Oliver and Pharr method was used in a previous study on the same machine-indenter by Franco et al.[8] in order to calibrate the indenter area function. Although the method adopted by Franco et al. gives good results, it requires the use of microscopy techniques, which also means that it is very difficult to implement at a small scale as well as time consuming.

It has been recently proposed that the P_m/S_u^2 parameter can be used in order to find the machine compliance and to calibrate the area function. However, it was only applied to the continuous stiffness measurement technique[10] and to fused silica[11] but not for a simple loading-unloading cycle and other materials. Research efforts have been made on the P_m/S_u^2 parameter and the most important variables that affect the Oliver and Pharr method using different materials, to provide the reasons why the iterative Oliver and Pharr method does not converge for Fischercope-indenter under study. The parameter P_m/S_u^2 allows the detection of potential problems in the machine calibration as well as performing the area function calibration, even for a very low compliance machine such as Fischecope. It suggests that it is a very important parameter. Given the importance of the iterative method, it will be briefly reviewed in this work, based on the works by Oliver and Pharr[3,11,12,14] and other publications[1,2,4,9].

2. Background

The analysis by the iterative method is applied to the unloading portion of the indentation cycle, assuming that the unloading behavior of the material is characterized only by elastic recovery. Figures 1 and 2 show the key parameters used in the analysis.

The method proposed by Oliver and Pharr allows for determination of the area function, which relates the cross sectional area to the

*e-mail: juan.meza@upb.edu.co

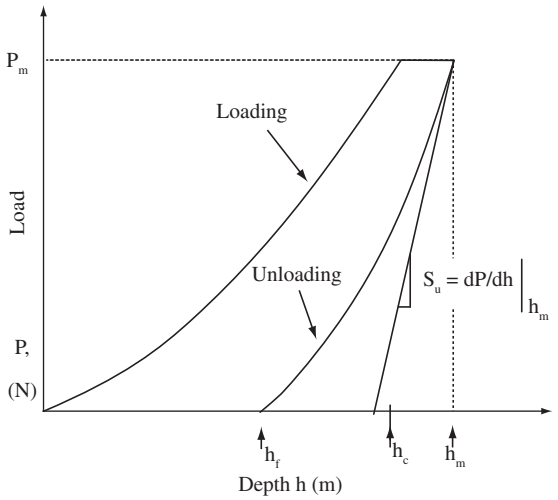

Figure 1. Schematic representation of indentation load-displacement data, showing the main parameters: P_m: peak indentation load; h_m indenter displacement at peak load; h_c contact depth; h_f final depth of the contact impression after unload and S_u initial unload stiffness[3].

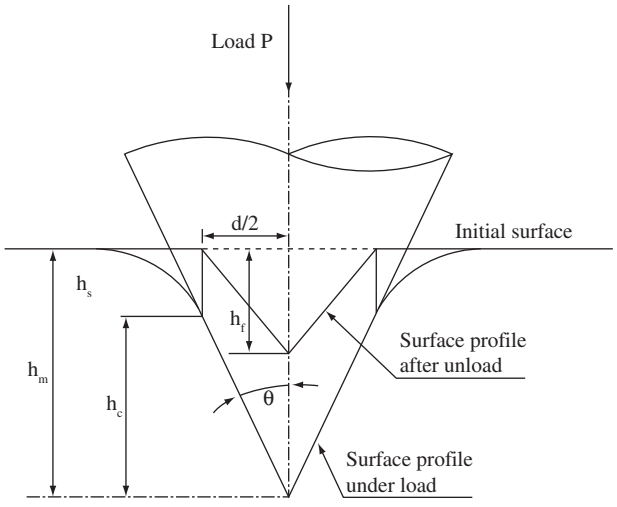

Figure 2. Schematic representation of the impression during load and impression left after unload, during a nanoindentation test[3]: h_s: distance form surface to the point of last contact between indenter and the specimen at maximum load; d: diagonal of contact.

distance from its tip, and the machine compliance. The method is based on the measurement of contact stiffness and does not require imaging of the indentation.

The method models the instrument and the specimen as two springs in series, in which case the machine compliance, C_f, and the specimen compliance, C_u, are related through the equation:

$$C_T = C_f - C_u \quad (1)$$

The specimen stiffness, S_u, can be calculated using the theory of elasticity[14] through the equation[14]:

$$1/S_u = C_u = \frac{\sqrt{\pi}}{2\beta E_r}\frac{1}{\sqrt{A_c}} \quad (2)$$

where β is a parameter which depends on the indenter geometry and material properties and usually takes a value from 1.00 to 1.08[11], but that have been demonstrated that it can take values as high as 1.26[15,16].

Also, E_r is the reduced modulus, which accounts for the elastic displacement of both the indenter and the specimen and is given by:

$$\frac{1}{E_r} = \frac{(1-\nu^2)}{E} + \frac{(1-\upsilon_i^2)}{E_i} \quad (3)$$

where E and ν are the elastic modulus and the Poisson ratio of the specimen, respectively. E_i and ν_i are the same parameters for the indenter.

After correcting the data by the machine compliance, the specimen stiffness, S_u, can also be obtained directly from the unload slope, as illustrated in Figure 1.

The procedure initially involves the conduction of high load indentations in a soft material, i.e high depths, such as aluminum. An estimate of the machine compliance and the area function can be obtained through an iterative procedure, which is listed below:

Load raw data.

Correct data: zero point reference (h_0) and thermal drift (Equation 4), where TD is the thermal expansion coefficient of the machine frame and t is the time:

$$h = h_t - h_0 - tD \times T \quad (4)$$

Fit unloading portion of load-displacement data to power-law relation, where K, h_f and m are fitting parameters:

$$P = K(h - h_f)^m \quad (5)$$

Calculate the total unload stiffness at maximum load:

$$S_T = \left.\frac{dP}{dh}\right|_{h=h_m} = Km(h - h_f)^{m-1} \quad (6)$$

Estimate the contact depth:

$$h_c = h_m - 0.75\frac{P_m}{S_T} \quad (7)$$

Estimate the contact area (A_c) through the ideal contact area (A_{cid}):

$$A_{cid} - 24.5h_c^2 \quad (8)$$

Estimate the machine compliance (C_f) and the indentation reduced modulus (E_r) by plotting C_T as a function of A_c:

$$\frac{1}{S_T} = C_T = C_f + \frac{\sqrt{\pi}}{2\beta E_r}\frac{1}{\sqrt{A_c}} \quad (9)$$

Calculate the corrected contact area:

$$A_c = \frac{\pi}{4\beta^2}\frac{1}{E_r^2}\frac{1}{(C_T - C_f)^2} \quad (10)$$

Adjust the contact depth as a function of the contact corrected area to Equation 11, where A_i are fitting parameters:

$$A_{O\&P} = A_0h_c^2 + A_1h_c + A_2h_c^{1/2} + ... + A_8h_c^{1/128} \quad (11)$$

Correct indentation data for the machine compliance:

$$h_{i+1} = h_i - PC_f \quad (12)$$

Using the new area function (Equation 11), the iterative calibration procedure is repeated several times until convergence is achieved

In Equation 7 the constant 0.75 is usually named ε and is a parameter which depends on the indenter geometry and material properties[3,11], and usually takes values from 0.72 to 0.78 for a Vick-

ers indenter. In addition, it is worth noting that after the first iterative cycle, the raw data is corrected by the estimated machine compliance. Therefore, the total stiffness, S_T, in Equation 7 is changed by the estimated sample stiffness, S_u.

The method follows by conducting a series of indentation measurements in a harder material, such as fused silica or sapphire, to obtain information at shallower depths, but in this case the machine compliance is the one previously obtained for the soft material (aluminum). The data produced for the soft and hard materials, contact depth, h_c, and contact area, A_c, are then used together to establish a unique area function for all depth levels.

After the projected contact area, $A_{O\&P}$, has been calculated through Equation 11, the hardness (H) is calculated as the maximum load, P_m, divided by $A_{O\&P}$ (Equation 13). The elastic modulus of the specimen, E, is calculated using Equation 9, with the reduced modulus, E_r obtained from Equation 3.

$$H = \frac{P_m}{A_c} \tag{13}$$

Although, the iterative O&P method has many advantages, its use has been limited for different reasons. Firstly, it is mathematically and time intensive. Secondly, C_f is subjected to large extrapolation and due to the significant dispersion in nanoindentation data, bias are created in the least squares estimative of the machine compliance, leading to an underestimation of its value[9]. The machine compliance can vary significantly from specimen to specimen, and may even depend on the location of the indentation in a single specimen[13]. Finally, the iterative method cannot be applied to materials that experience pile-up, since, in this case, the actual contact depth and the actual contact area would be larger than those predicted by this method, which results in an overestimation of both hardness and elastic modulus[13,17-19].

Other techniques for determining the area function and machine compliance include imaging of the residual imprints by optical microscopy, scanning electron microscopy[13], transmission electron microscopy[2] or atomic force microscopy[20,21]. In these cases, the area function can be obtained by fitting the imaged areas as a function of the contact depths computed from the indentation load-displacement data to Equation 9. However, optical and scanning imaging of small indentations is very difficult. Transmission electron microscopy imaging requires the use of replicas, besides being a technique that is both expensive and time-consuming[3]. Another option refers to the topographic characterization of the indenter through atomic force microscopy; however, it is also time consuming and requires large investments in terms of equipments and optical-laser sensors[5].

The iterative method can be simplified if reference materials with known elastic modulus are used; a technique defined as the Constant Modulus Method. These known values allow the method to converge to the machine compliance, C_f, more quickly. Once the machine compliance, C_f, is known, there is no need for iteration in other materials.

Another alternative method was recently developed by O&P[11], based on an earlier idea of Joslin and Oliver[22], that the ratio of the load to the stiffness squared (P_m/S_u^2) can be used to determine the ratio H/E^2 without the need of determining the indenter area function. According to O&P[11], this method, defined in which follows as the *Constant Hardness and Constant Elastic Modulus Method*, is valid provided that the hardness and elastic modulus of the specimen do not vary with depth. Other authors have used similar ideas[4,23,24]. To explain this method, it is useful to rewrite some of the equations used above. Equations 9 and 13 can be combined as:

$$C_T = C_f + \frac{\sqrt{\pi}}{2\beta}\frac{1}{E_r^2}\frac{\sqrt{H}}{\sqrt{P_m}} \tag{14}$$

which can also be written as:

$$A_c = \frac{\pi}{4\beta^2}\frac{P_m}{E_r^2\dfrac{P_m}{S_u^2}} \tag{15}$$

and also as:

$$\frac{P_m}{S_u^2} = \frac{\pi}{4\beta^2}\frac{H}{E_r^2} \tag{16}$$

The Constant Hardness and Constant Elastic Modulus Method is organized as follows: A plot of C_T as a function of $1/\sqrt{P_m}$ provides C_f as the intercept and the slope is related to the hardness and the reduced modulus (Equation 14). Note that under these conditions, there is no necessity of knowing the area function a priori, neither of an iterative procedure, however, the use of Equation 14 has the same large extrapolations problems than Equation 9. The Constant Hardness and Constant Elastic Modulus Method follows correcting the raw data by a value of $-PC_f$ (Equation 12), which allows the calculation of the unload specimen stiffness, S_u, at different loads. In practice, to obtain the machine compliance, only indentations in reference materials, obtained at high loads must be used, in order for the effect of the tip roundness to be negligible and, therefore, for hardness to be constant.

Then, Equation 7 (with S_T substituted by S_u) and Equation 15 provide the contact depth, h_c, and the contact area, A_c, respectively. At this point, a non linear weighed least square fitting procedure between h_c and A_c, to a function with the characteristics of Equation 11, provides the area function.

In addition, once C_f is established, the ratio P_m/S_u^2 is a directly measurable experimental parameter, since S_u is determined form the slope of the unloading data (Equation 6) and P_m corresponds to the maximum applied load in the indentation test. According to Equation 16, the ratio P_m/S_u^2 must be constant (a material property[11]), since it depends only on E_r and H, and both quantities are assumed constant. Therefore, a plot of the ratio P_m/S_u^2 as a function of depth or load, must be a flat curve, at least at high loads (or depths), where the indenter tip has no effect on the hardness. Thus, the ratio P_m/S_u^2 provides a manner to corroborate if the value of the machine compliance is correctly assessed[11].

The calculated value of P_m/S_u^2 can also be compared with theoretical ones, but care must be taken in the hardness value that will be used, because the contact area measured in nanoindentation tests is the area at maximum load, defined by the indentation contours, rather than by the diagonals[11,13,25].

Although, the idea of using the ratio P_m/S_u^2 to corroborate the accuracy of the machine compliance was recently developed by Oliver and Pharr, no other works have explored it.

In this work, the applicability of the different methods for the calibration of the machine compliance and calibration of area function was initially investigated based on measurements conducted on different materials. In particular, it was analyzed if the procedure described above for the Constant Hardness and Constant Elastic Modulus Method provides values of area function and machine compliance comparable with those provided by other methods.

In addition, the effect of tip radius on the ratio P_m/S_u^2 was also studied. Other issues related to initial contact depth, thermal drift, contact stiffness, unloading curve and tip roundness are also discussed.

3. Experimental Procedure

3.1. Materials

The materials analyzed in this work are shown in Table 1. Fused silica was chosen as a reference material, due to its well known proper-

ties and homogeneous structure. Polycrystalline sapphire, aluminum (1100), glass (standard reference material provided by Fischerscope), steel (standard reference material with 695 HV), high purity copper and polycrystalline titanium were also used. The aluminum specimen was mechanically polished and finished until 0.025 μm with silica colloidal with the aim of eliminating mechanical hardening. This procedure was conducted in accordance to the work by O&P[3], although it is recognized that electropolishing would probably be more efficient in removing all mechanically worked material.

The elastic modulus values reported for materials in Table 1 was measured by standard acoustic methods[26] and the other values in Table 1 were extracted from the literature.

3.2. Equipment and indentation procedure

Indentations were conducted on a Fischerscope H100V depth-sensing machine, manufactured by Helmut Fischer GmbH and equipped with a Vickers diamond indenter. In this work, care was taken in order to analyze indentation tip roundness and its effects on the results.

A schematic representation of the head of a Fischerscope H100V machine is shown in Figure 3. It is possible to observe that this machine has a reference ring.

A series of indentations were conducted following the sequence shown in Figure 4, with load values between 10 and 1000 mN. In each loading and unloading cycle, 200 data points were acquired in steps of 0.1 s at a constant dP/dt ratio. Although this equipment is also capable of applying the load according to a "Squared law", constant $d\sqrt{P}/dt$[27], the latter was avoided. After loading, a dwell time of 30 s at the peak load was used for the harder materials and 60 s were selected for the softer materials, with the aim of reducing creep effects[28]. A dwell time of 30 s was also implemented at the end of the unloading step in order to evaluate thermal drift effects[3,7,25,28].

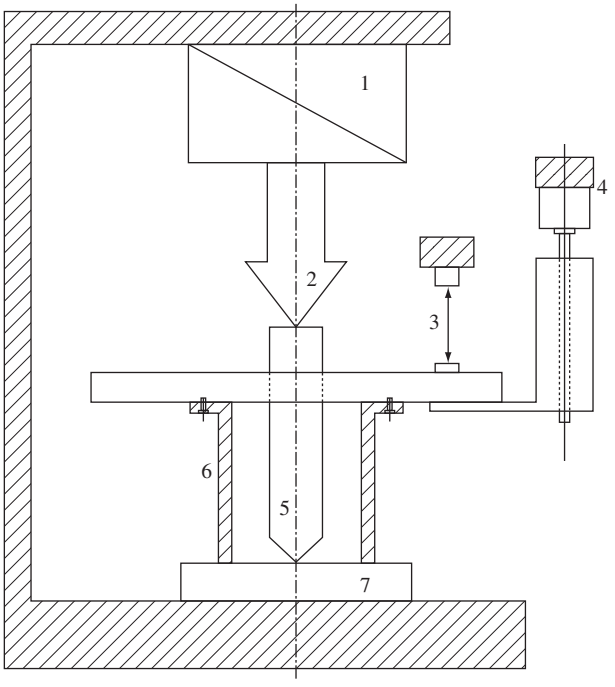

Figure 3. Schematic representation of head system measurement of a Fischercope H100V machine: 1) electro-magnetically load system; 2) force; 3) displacement sensor; 4) motor; 5) indenter; 6) reference ring; and 7) specimen[27].

It is important to mention that the Fischerscope H100V equipment does not allow the application of a series of loading-unloading cycles to minimize the reverse plastic effects during the last unload cycle. However, Simões[28] has demonstrated, in a similar machine, that the dwell time at maximum load is also efficient in this regard.

At least, eight indentation curves were obtained for each value of maximum load and only the five within two standard deviations from the average P_m/S_u^2 ratio were used in the analysis. After the series of indentations in each specimen, the indenter was cleaned by impregnation with drop of alcohol and conduction of an indentation in Polymethyl methacrylate, PMMA, which, due to its electrostatic action, helps with the removal of adhered particles.

The zero-point for the measurement of the load-displacement curve, which is affected by specimen roughness[29] and other machine and software parameters[1,25], was obtained by a polynomial fitting of the first fifteen data points of indentation depth during loading, followed by the extrapolation to zero load[25].

For the aluminum specimen, the residual imprints at high maximum loads (from 50 to 1000 mN) were measured by direct observation in an optical microscope *BX60M Olympus*, equipped with a Leica image analysis software. For all materials, the diagonals of the

Table 1. Materials used in indentation studies. Elastic modulus and poisson' ratio were measured by acoustic methods except for sapphire and titanium specimens.

Material	E (GPa)	HV0.1 (GPa)	Poisson ratio
Fused silica[(a)]	72.90 ± 0.52	6.7	0.160 ± 0.008
Aluminum (1100)	67.90 ± 1.95	0.27	0.356 ± 0.007
Sapphire	430 – 460[(b)]	18	0.21 – 0.27[(b)]
Glass[(c)]	72.50 ± 0.42	5.2	0.230 ± 0.005
Steel[(d)]	212.50 ± 1.22	6.8	0.280 ± 0.002
Copper 99.99%	116.6 ± 0.1	1.1	0.360 ± 0.001
Titanium 99.99%	107.0 – 112.5[(b)]	1.95	0.340 – 0.354[(b)]

[(a)]Standard calibration sample from CSM instruments; [(b)]Values obtained from CES EduPack Software R; [(c)]Standard calibration sample from Helmut Fischer GmbH; and [(d)]Asahi Oio Hyogo Japan standardized block for hardness 700 HV Buehler Ltd ISO 4547,

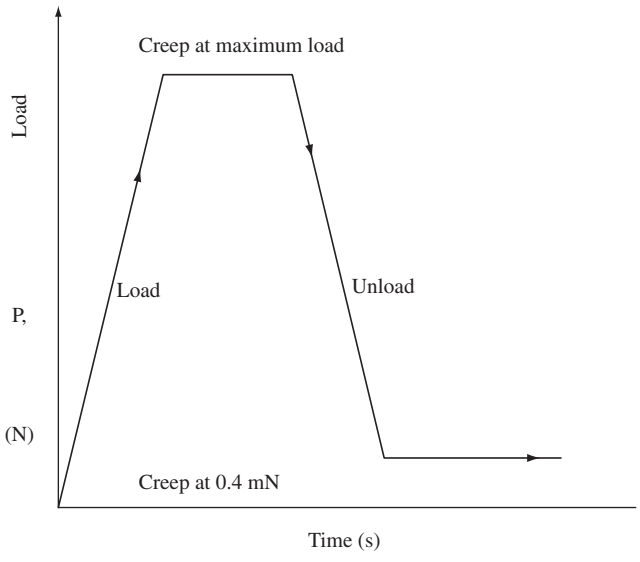

Figure 4. Load-time sequence of the instrumented indentation tests.

residual impressions obtained at a maximum load of 1000 mN were used to calculate the Vickers hardness values presented in Table 1.

4. Results and Discussion

4.1. Zero reference contact point and thermal drift

The reference ring (Figure 3) provides the advantage of acquiring a first reference point during an indentation, and, consequently, a better precision in setting the zero reference point. The Fischerscope equipment detects the zero reference point by extrapolation from the first three incremental load steps[27]. However, although very low loads are applied in this initial contact stage, little penetration will always be present and must be taken into account[25]. Figure 5 shows a typical plot of the initial load data obtained for fused silica. In all specimens under study, corrections for this initial penetration were always lower than 5 nm, which demonstrates the advantage of the reference ring in setting the zero reference point.

Another advantage of this ring is related to the thermal drift. Following the results obtained by Simões[28], only the data after 20 s of creep at 0.4 mN were used to calculate the thermal drift coefficients, which always resulted in values lower than –0.3 nms^{-1}. This value is in the same order of magnitude of that of the newer instruments, which are designed with better materials, i.e., materials with lower thermal expansion coefficient than those in the Fischerscope[25]. The fact that thermal expansion is low in the Fisherscope equipment is due to the fact that the ring moves together with the measurement head, thus compensating elastic recoils, such as those due to frame compliance and thermal drift.

4.2. Unloading data

In theory, if the material hardness is constant, a linear dependence will exist between dh/dt and $d\sqrt{P}/dt$. For this reason, some machines are designed with the possibility of maintaining the ratio $d\sqrt{P}/dt$ constant (i.e., constant deformation rate), as in the case of Fischerscope machines. Figure 6 shows the difference between acquiring the data with constant $d\sqrt{P}/dt$ ratio and with constant dP/dt ratio, in the unloading portion close to the maximum load of the load-unload cycle. It is clear that when a constant $d\sqrt{P}/dt$ ratio is used, less data is acquired close to the maximum load. This fact occurs because at high depths the contact stiffness rises and large increases in load are required to obtain little increase in depth. Therefore, since this part of the unload curve is the one selected to provide the unload stiffness, a less precise measurement of S_u is obtained when constant $d\sqrt{P}/dt$ is used, in comparison with the data obtained with constant dP/dt ratio. Therefore, in this work constant dP/dt ratio was selected during the load-unload cycles.

Figure 7a shows the variation of the unload stiffness as a function of the portion of the unload curve used to analyze unload data, for different values of peak load. These values were obtained by fitting the unload data to Equation 5. Figure 7a indicates that, for fused silica, results were only slightly susceptible to the portion of the unload data chosen, particularly when less than 50% was selected. However, parameters such as h_f and *m* (Equation 5) were highly dependent on the unload portion, as illustrated in Figure 7b,c. It is worth to mention that h_f diminished with the unload portion down to unrealistic values, which is a result of the mathematical fitting, especially for materials with low h_f/h_m ratio, i.e, those with high elastic recovery during unloading. In this work, 50% of the unload data was adopted for the analysis.

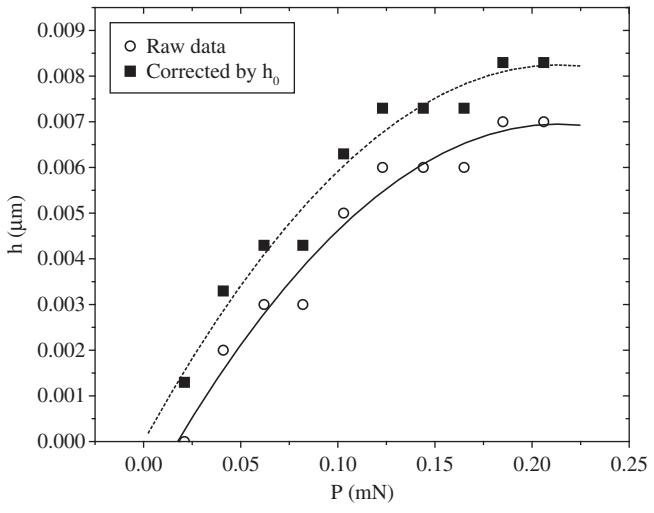

Figure 5. Initial depth correction for fused silica.

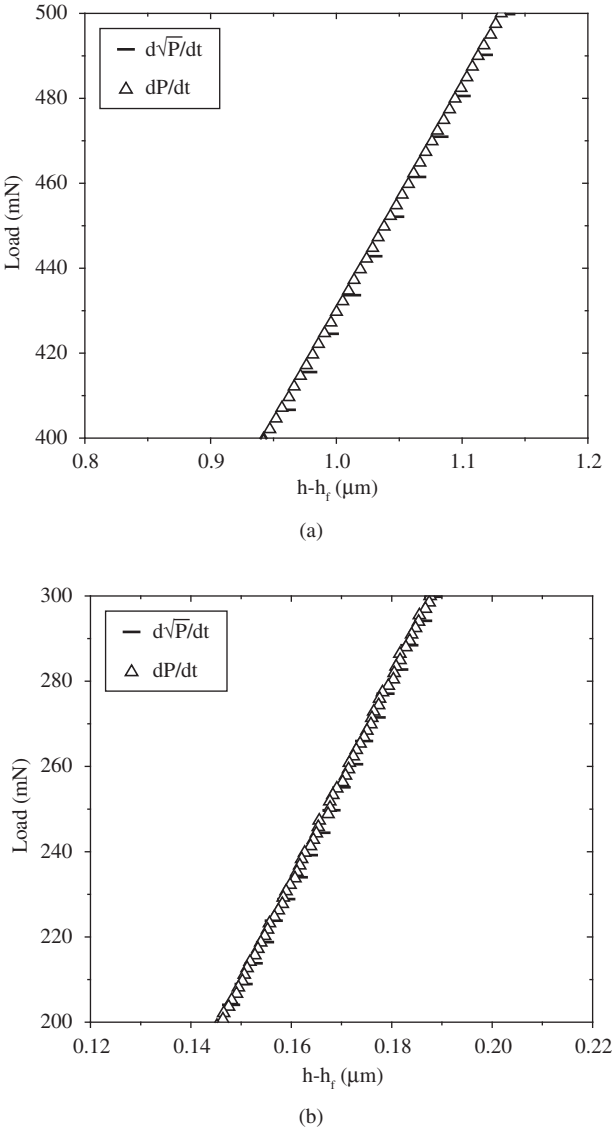

Figure 6. Unloading data acquired for a) fused silica; and b) aluminum close to maximum loads of 500 mN (constant $d\sqrt{P}/dt$ ratio) and 300 mN (constant dP/dt ratio) respectively.

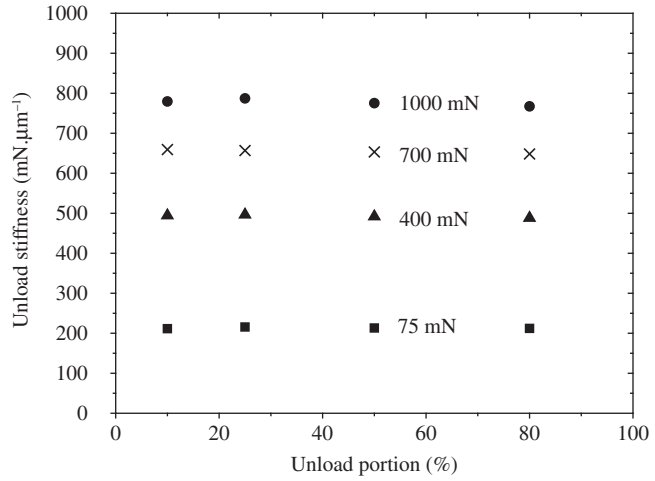

(a)

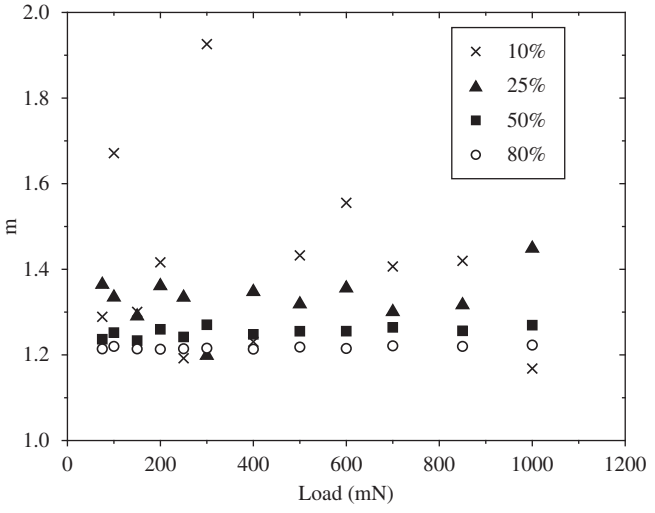

(b)

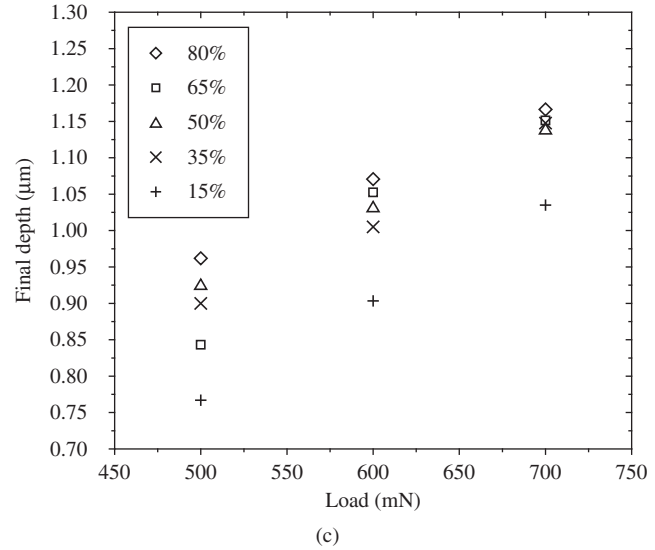

(c)

Figure 7. a) Unloading stiffness S_u; b) m constant of Equation 5; and c) final unloading depth h_f, as function of both the peak load, P_m, and the percentage of the unload data respect the maximum load used to obtain these parameters for fused silica.

4.3. Machine compliance

4.3.1. Machine compliance through constant hardness and elastic modulus method

The iterative O&P method did not converge when both C_f and E_r were unknown, neither when the elastic modulus was substituted for the one measured by acoustic methods.

As explained in Sec. 2, through the Constant Hardness and Constant Elastic Modulus Method, a plot of C_T as a function of $1/\sqrt{P_m}$ (Equation 14) provides the machine compliance as the intercept. This procedure was implemented, and results are shown in Figure 8.

For fused silica, the use of the data obtained at loads above 800 mN was avoided due to the propagation of lateral cracks, as shown in Figure 9. This extensive damage of the surface probably affected the shape of the unload curve[25]. Figure 8 indicates that, even when the specimens were tested in the same region of the XY stage, the values of the machine compliance were not unique. When testing glass, fused silica and sapphire, values were equal to 0.045, 0.028 and 0.001 nm.mN^{-1}, respectively (Figures 8a,b,c). Standard errors are reported on Figure 8.

An important issue with respect to machine compliance is the clamping of the specimen onto the XY stage by the reference ring, as explained in Sec. 4.1. Since the measuring head travels together with the reference ring, the machine hardly suffers deformation and, consequently, the measured compliance will be lower compared with that of other types of equipment; typically ten times higher (see values reported in Sawa[6] for various machines).

It is important to add that, in the literature, the value of C_f obtained for a similar machine was approximately equal to 0.04 nm.mN^{-1} [4,7], which is close to the values obtained in present work, for glass and fused silica (Figures 8a,b).

Figure 8d indicates that the value of machine compliance calculated for the aluminum specimen was different from those calculated for the other specimens. This result is probably associated to a hardened layer on the aluminum specimen, in spite of the care taken during preparation. This hardened layer was confirmed by calculation of hardness values measured as the maximum load divided by either the corner to corner area (A_{CC}) or the real contact area inside indentation borders (A_r) (Figure 10), both based on measurements conducted with the Leica image analysis software. This variation in hardness precludes the use of the Constant Hardness and Constant Elastic Modulus Method for the evaluation of the machine compliance.

For the aluminum specimen, the intercept of the graph of C_T as a function of $1/\sqrt{P_m}$ provided a value of machine compliance of –0.013 nm.mN^{-1}, Figure 8d. The accuracy of the calculated value of C_f was assessed in the following manner: The second right hand term of Equation 14, i.e., the slope of C_T vs. $1/\sqrt{P_m}$ (Figure 8d) is related with the hardness H and the elastic modulus E. Therefore, any E or H can be found, provided one of them is known. In this work, both were known. The elastic modulus is reported in Table 1 (67.9 GPa) and the true hardness is reported in Figure 10, being equal to 0.27 GPa. Using the hardness and the slope of Equation 14, an elastic modulus of 63 GPa was obtained, which is 8% lower than the expected value (67.9 GPa). Thus, due to the aluminum hardened layer, the use of a measured value of hardness did not provide the measured value of elastic modulus, which suggests that the C_f value reported in Figure 8d is incorrect.

4.3.2. Machine compliance: direct imprint measurement method with the aluminum specimen

Since the constant hardness method did not work properly for the calculation of C_f for the aluminum specimen, the procedure of plotting the contact compliance C_T as a function of $1/\sqrt{A_c}$, with A_c measured by imaging methods (Equation 9), was implemented[2,13]; this

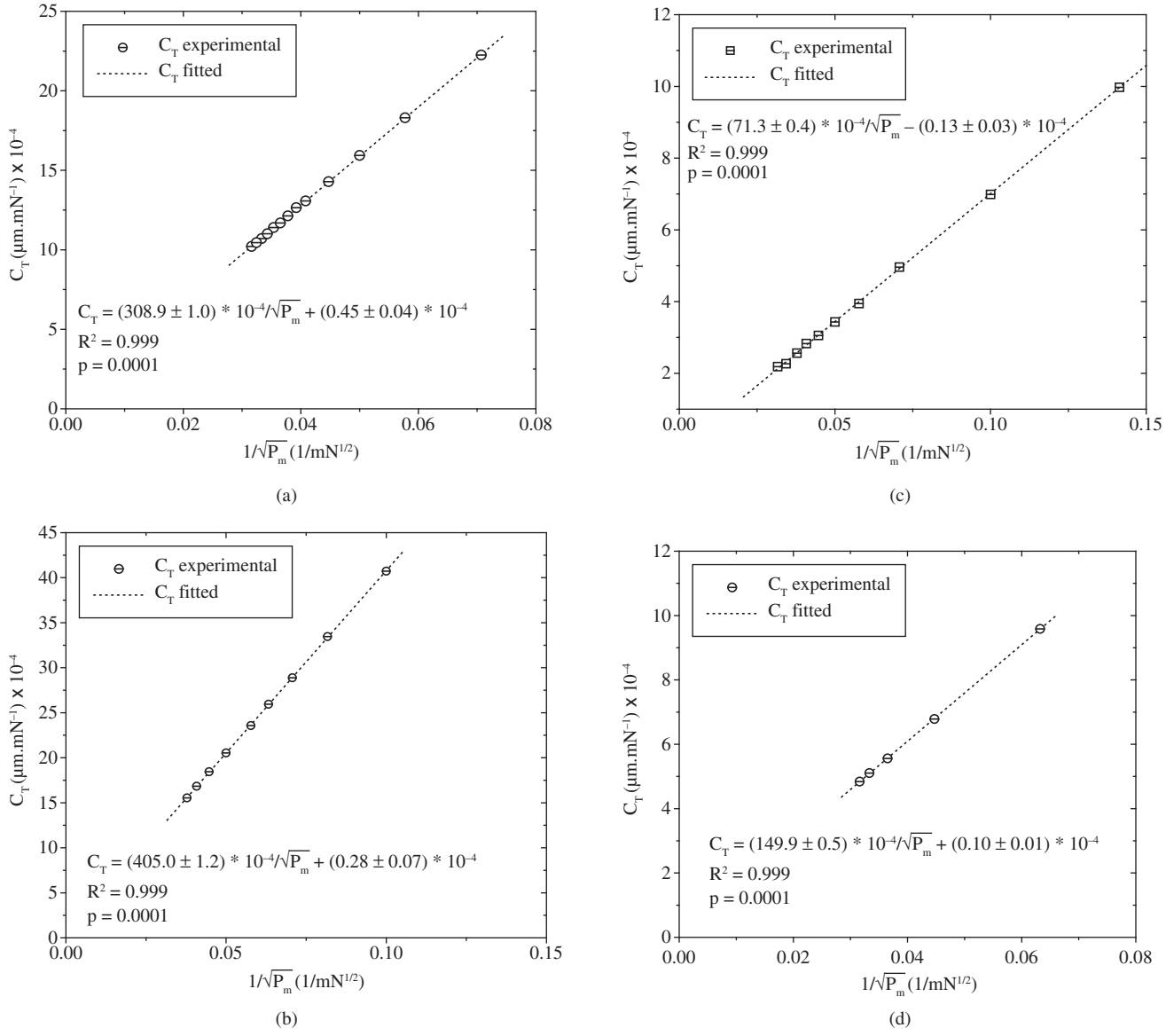

Figure 8. Variation of total compliance C_T as function of $1\sqrt{P_m}$ for: a) glass; b) fused silica; c) sapphire; and d) aluminum samples.

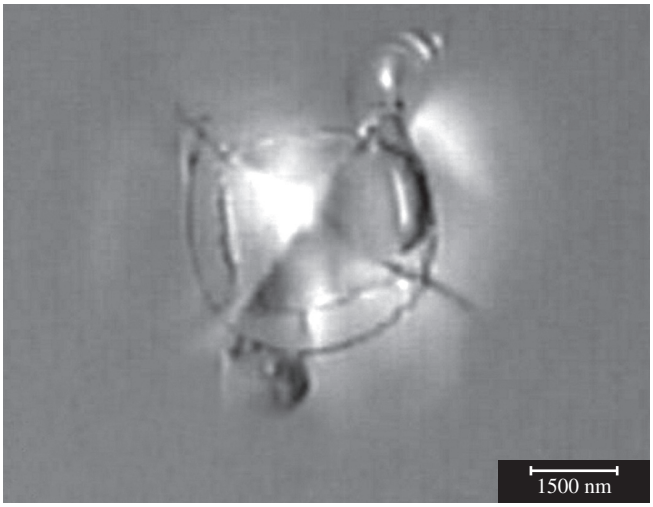

Figure 9. Indentation on fused silica at 1000 mN, showing the lateral cracks that have emerged to the surface during unload.

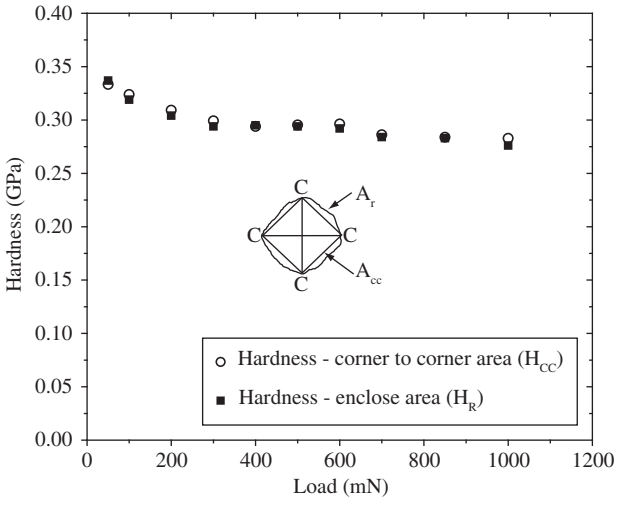

Figure 10. Hardness as a function of load for aluminum, calculated using corner to corner area (H_{CC}) and real projected area (H_R).

method is referred as direct imprint measurement method. This kind of plot is shown in Figure 11 for the aluminum alloy. It is possible to observe that both the corner to corner (i.e. the one calculated as the diagonal squared) and real contact (i.e. the one calculated by means of the borders of the impression) areas produced similar results. However, the values of the real contact area must be employed in order to reduce the effect of material deformation (pile-up/sink-in). In this case, a machine compliance of 0.004 nm.mN^{-1} and a slope of 1.265 x 10^{-4} were obtained. The accuracy of the calculated C_f was proved in a similar manner to that employed in Sec. 4.3.1, but using Equation 9. In this case, an elastic modulus of 67 ± 1 GPa was obtained, which is close to the expected one. Thus, in the case of the aluminum specimen the direct imprint measurement method provided a result in better agreement with the expected one.

4.4. Ratio of load to the stiffness squared (P_m/S_u^2)

Figure 12 shows the ratioP_m/S_i^2 (before C_f correction) and also the ratio P_m/S_u^2 (after C_f correction) for each one of the materials studied in Sec. 4.3.1. The C_f values used for fused silica, glass and sapphire, were

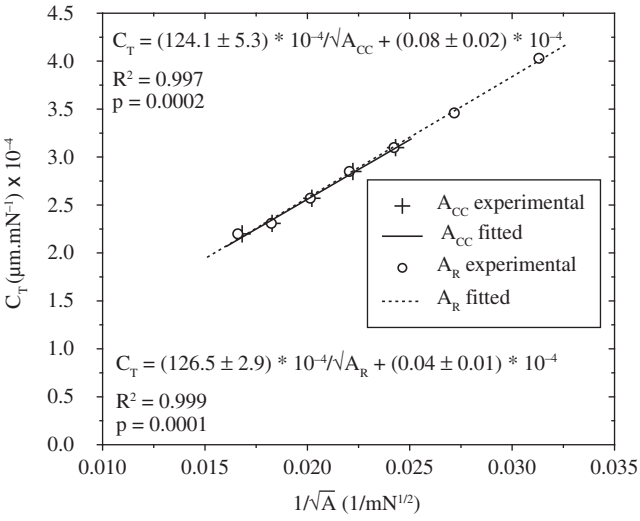

Figure 11. Variation of the total compliance C_T against $1/\sqrt{A_c}$ for aluminum.

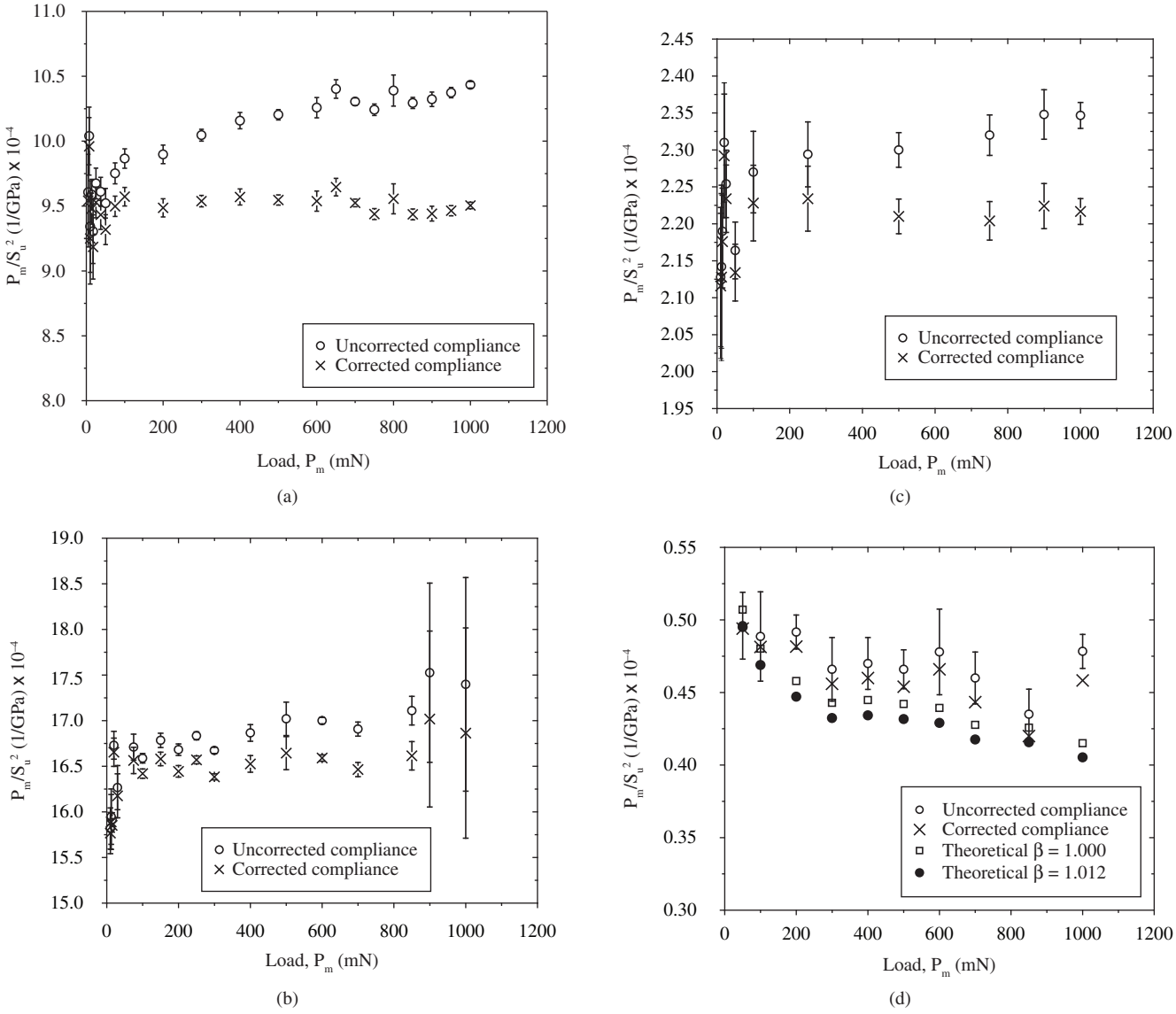

Figure 12. Variation of the P/S^2 ratio for the uncorrected machine compliance C_f vs. the maximum load for a) glass; b) fused silica; c) sapphire; and d) aluminum.

those found by the Constant Hardness and Constant Elastic Modulus Method in Sec. 4.3.1 (Figures 8a,b,c), while for aluminum the value was that found by the direct imprint method Sec. 4.3.2 (Figure 11). As stated in Sec. 2, to assess the accuracy of the calculated machine compliance, the ratio P_m/S_u^2 must remain constant at relative high loads, which allow avoiding effects of tip roundness on this parameter[11]. This is not the same case when Equation 9 is used to find out C_f, because, as it was proved by Suganuma et al.[10], tip roundness still plays an important role on the contact area even at high depths. Then, C_f values found in Figure 8 which assumes a P_m/S_u^2 constant ratio as is verified on Figure 12, for fused silica, glass and sapphire, will be only influenced by experimental errors and for extrapolation of the adjusted data to zero. Thus, results shown in Figure 12 for these materials lead to the conclusion that the machine compliances were, within experimental error, correctly assessed in each of these three cases. The values of P_m/S_u^2 for fused silica, sapphire and glass at high depths were 0.00165, 0.000220 and 0.00095 GPa^{-1}, respectively, with a standard deviation less that 3%. Thus, it can be concluded that the machine compliance also depends on the sample mounting, which can be due in part to the reference ring system, because depending on the mechanical properties of the material it could slightly deform the surface sample in which it is sitting on.

Figure 12b also shows that for the fused silica there was an increase in both the value and standard deviation of the ratio P_m/S_u^2 at loads greater than 800 mN, (Figure 12b), which is probably due to the extensive damage of the specimen surface (Figure 9), as explained in Sec. 4.3.1.

It is instructive to compare the theoretical results of the ratio P_m/S_u^2 (calculated using the right had side of Equation 16 with those obtained experimentally (directly from the unload slope and maximum load). Considering that in literature the hardness values reported for fused silica vary from 8 to 10 GPa[25] and that its reduced elastic modulus E_r is about 69 GPa, and assuming a β value of 1.012, the theoretical P_m/S_u^2 values for this material, would be between 0.00127 and 0.00158 GPa^{-1}. Values in this range were reported, for example, by Oliver and Pharr[11] (0.0015 GPa) and also by Fischer-Cripps[25] (0.00145 GPa^{-1}, obtained using H = 9.45 GPa and β = 1.034 for Berkovich indenter). In the present work, the experimental value of the ratio P_m/S_u^2 for fused silica was 0.00165 GPa, for loads ranging from 75 to 700 mN, Figure 12b, which is out of the theoretical range. In order to explain this difference, it is necessary to observe that the literature generally reports that loading and unloading curves are only a function of indenter geometry and elastoplastic properties. However, from the investigations of Cheng and Cheng[30,31], based on dimensional analysis for a perfectly rigid indenter, they proved that the load behavior also depends on the indenter tip roundness, according to Equation 17:

$$P_{load} = Eh^2\Pi_L(Y/E, h/R, \nu, \eta, \theta) \quad (17)$$

Besides, it is also possible to prove that the unload behavior follows Equation 18[32,33]:

$$P_{unload} = Eh^2\Pi_U(Y/E, h/h_m, h/R, \nu, \eta, \theta) \quad (18)$$

In Equations 17 and 18 Π_L and Π_U are dimensionless functions of: the yield strength Y, the elastic modulus E, the indenter tip radius R, the Poisson's ratio ν, the hardening index η, the indenter angle θ, the load P, the depth h, and the maximum depth h_m.

Using Equations 17 and 18, we have recently proved that[33]:

$$\beta = \Pi_\rho(R/h_m, \nu, \eta, \theta) \quad (19)$$

This equation shows that the β factor depends on indenter geometry, the ratio R/h_m, and some of the specimen mechanical properties. This dependence explains why, in order to obtain a correct hardness or elastic modulus, the β factor must be modified depending on the tip roundness-material combination, as reported by Troyon[15,16]. For example, higher values of β may lead to a decrease in the theoretical ratio P_m/S_u^2 [15,16]. In this work, a value of β of about 1.045 would produce values of ratio P_m/S_u^2 approximately equal to 0.0015 GPa^{-1} for fused silica, which is on the expected range. On the other hand, such high value of β would produce higher hardness values (Equations 16), which, in our case, would be of approximately 11 GPa, for fused silica, which is a slightly high in comparison with common literature reported values.

Figure 12d shows a different situation in the case of the aluminum specimen. This behavior is explained by its variation in hardness. As indicated in Figure 10, higher hardness values were obtained for the aluminum specimen at lower loads. Therefore, at lower loads, Equation 16 predicts an increase in the ratio P_m/S_u^2. Figure 12d also shows that, contrary to the case of fused silica, the value of β must be equal to 1, i.e, less than the theoretical one (1.012), in order for the calculated value of P_m/S_u^2 to be close to the theoretical one.

Although the results have shown that the machine compliance must be established according to the mounting sample, in the Fischerscope H100V machine the omission of this correction does not impose significant errors in the results, because C_f is very low. For example, in the worst cases, at the highest load (1000 mN), for sapphire and aluminum, the error in the contact depth is of about 0.2 and 0.03%, respectively, which are negligible considering that the indentation techniques are characterized by a relatively high dispersion in the results[9].

As the indenter has a tip radius of 1.33 μm, some parameters could be affected by the depth/tip radius ratio particularly at low values of it, as is the case for the β factor. This is one of the reasons why we avoid in our analysis the first 150 nm. However, according to ref. 10, the contact depth is not influenced by the maximum depth/tip radius (See Figure 7 in ref. 10). Thus the area function can be already determined according to the O&P procedure as illustrated in next section.

4.5. Area function

Figure 13 indicates that an indenter with a tip radius of approximately 1.33 μm, was used in all indentations. Figure 13 also shows some transferred particles of aluminum after indenting; particles that were eliminated by the careful procedure described in Sec. 3.2. The following paragraphs will discuss other implications of this high tip roundness, as well as two methods to calculate the area function of this rounded tip indenter.

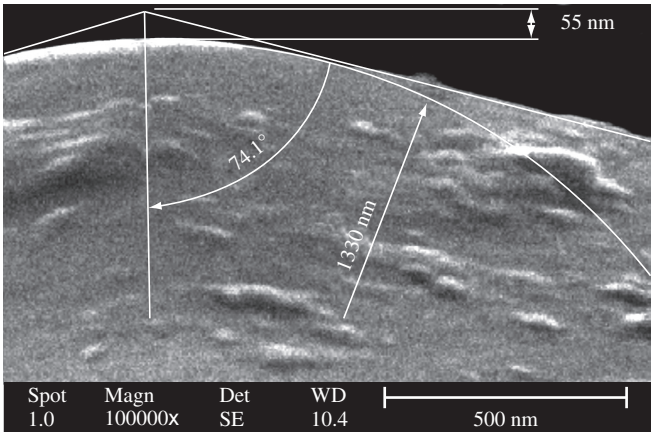

Figure 13. High magnification of the blunt indenter Vickers tip.

4.5.1. Iterative O&P method

The iterative O&P method was applied to find both the machine compliance and the elastic modulus of all the materials studied above, but the method did not converge in any case. Even when the correspondent elastic modulus was substituted in the respective equations, i.e. when the O&P Constant Elastic Modulus Method was used, the convergence to C_f was not obtained. Three explanations are possible in this case. First, the machine compliance is very low and, therefore, is very sensitive to the large extrapolations involved in Equation 9. Second, even at relative high depths, the relatively large tip radius leads to higher values of the first estimated ideal contact area, in relation to the real area[10]. In other words, the slope of Equation 9 will be much higher than the ideal one and, therefore, the first elastic modulus will be overestimated. Third, the dependence of β factor on the ratio R/h_m is accentuated at low depths. With the rounded tip used in present work, this influence possible extent until considerable depths. Therefore, under these conditions the iterative O&P method will hardly converge.

4.5.2. Constant modulus and constant hardness method

An alternative procedure was implemented, based on the assumption that the hardness and the elastic modulus are constant and known[11]. After correction of the data by initial depth, thermal drift and machine compliance, as established in Sec. 4.3, the contact area was calculated based on Equation 15 for each contact depth, using the standard glass calibration specimen and a β factor equal to 1.012. Later on, a non linear least square interpolation of these data to (Equation 11), weighed by the inverse of the maximum depth[25], was conducted and led to the area function shown in Equation 20, in which h_c is in μm:

$$A_{O\&P} = 24.62843716129h_c^2 + 5.0537296069h_c + 0.6484499427h_c^{1/2} \quad (20)$$

Equation 20 is valid for depths higher than 150 nm. This distance is higher than the transition distance from the rounded part of the indenter to the straight sides of the indenter. Under 150 nm, Equation 20, produces a high dispersion, which is probably due to a combination of specimen surface roughness and to the fact that the rounded tip shape is not perfectly spherical.

4.6. Hardness and elastic modulus

To assess the validity of the area function presented in Equation 20, copper, steel and titanium specimens were also tested at different loads. A machine compliance of 0.02 $nm.mN^{-1}$ was used in these cases (an average of the compliances obtained for aluminum, fused silica, sapphire and glass). The values of the hardness and elastic modulus of these materials are shown in Figures 14 and 15. A comparison of elastic modulus values with those on Table 1, indicates that the area function obtained in this work, in conjunction with the assumed machine compliance, produced measurements with differences lower than 6% for all materials, except for sapphire, for which the measured value presents a difference lower than 10% with respect to the expected one. However, a close inspection, for example in the case of fused silica, shows mean values of 68.13 ± 0.5 for its elastic modulus and 9.2 ± 0.18 for its hardness. The difference of the obtained elastic modulus 68.13 with respect to that measured by acoustic methods 72.9 can be explained by the fact that the β factor used in this work (1.012) is less than the true value for this material, as discussed in Sec. 4.4.

5. Conclusions

The ratio P_m/S_u^2 proved to be a very helpful parameter to assess the quality of the analysis of depth-sensing indentation data; to obtain

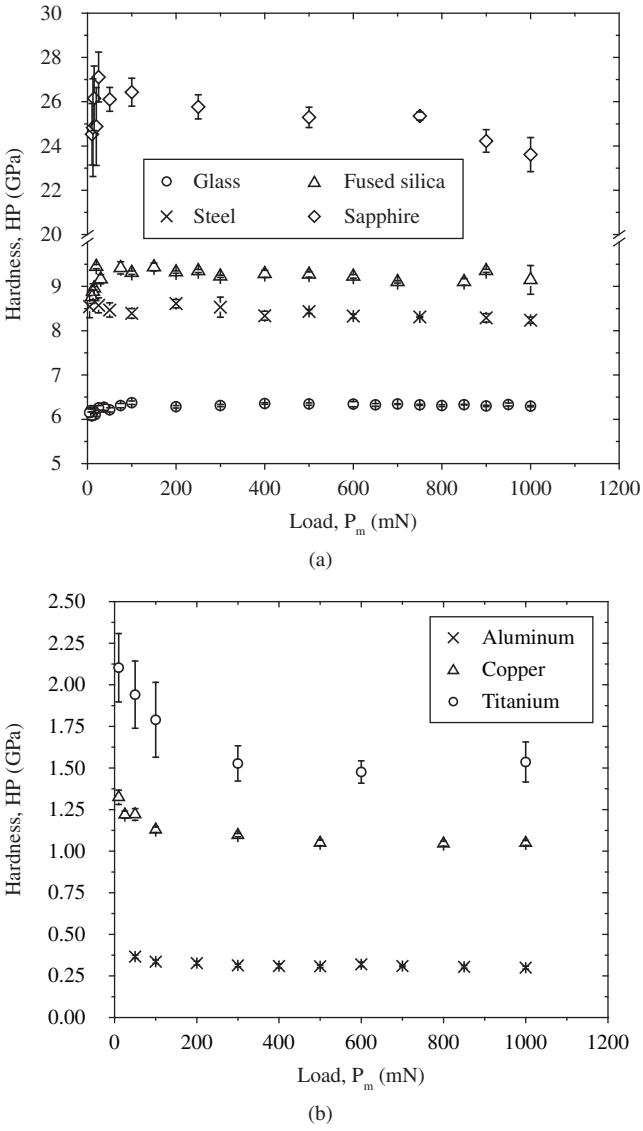

Figure 14. Hardness values vs. the maximum load for the tested materials.

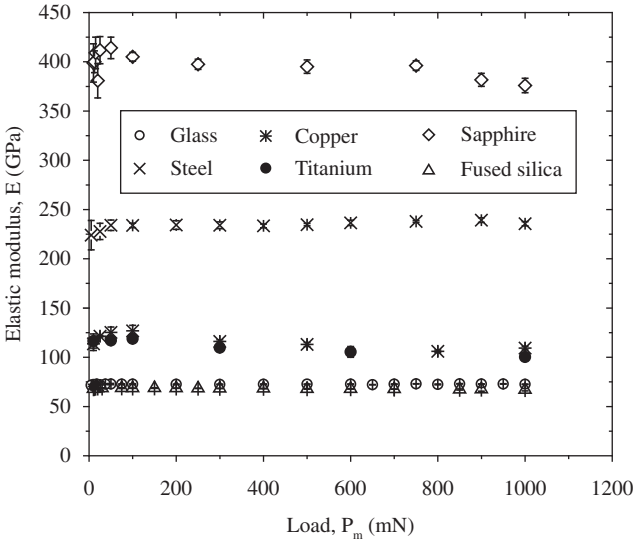

Figure 15. Elastic modulus values vs. the maximum load for the tested materials.

the area function and to verify if machine compliance was correct assessed. This ratio can be used to study conventional nanoindentation machines without CSM capability. However, results suggest that this parameter could be not strictly a material parameter due to possible influences by the tip roundness of the indenter. Taking into account that β factor also varies depending on the material and on the tip roundness, the area function calibrated with a reference material is always biased for other materials. However, this deviation was lower than 6% for the majority of the materials and the machine studied in this work.

Results obtained in this work have shown that good calibrations of the area function are possible, even if a highly rounded tip indenter is used.

The fused silica standard specimen, commonly used to calibrate nanoindenter machines, must be employed with caution at high load levels, due to the extensive damage produced, characterized by lateral cracks that emerge to the specimen surface during unload, affecting the contact unload stiffness.

A detailed study on a Fisherscope H100V machine confirmed that machine compliance varies depending on the sample mounting. Therefore, if accurate measurements must be obtained, this compliance needs to be established for each material under study, each time that a test is performed. However, since the machine compliance is low, errors lower than 0.2% in contact depth were obtained in this work.

Similar to the machine compliance, thermal drift and initial contact depth also resulted in little impact in the results. This is due to the reference ring incorporated in the machine, which travels with the specimen and protects the indentation zone from the surrounding environment.

Acknowledgments

The authors would like to acknowledge the support for this research provided by the Instituto Colombiano para el Desarrollo de la Ciencia y la Tecnología 'Francisco José de Caldas' (COLCIENCIAS), by National doctoral grant program and by The State of Sao Paulo Research Foundation (FAPESP).

References

1. Fischer-Cripps AC. Review of analysis methods for sub-micron indentation testing. *Vacuum.* 2000; 58(4):569-585.
2. Doerner MF, Nix WC. A method for interpreting the data depth-sensing indentation instruments. *J. Mater. Res*. 1986; 1(4):601-609.
3. Oliver WC, Pharr GM. An improved technique for determining hardness and elastic modulus using load and sensing indentation experiments. *J. Mater. Res*. 1992; 7(6):1564-1583.
4. Seitzman L. Mechanical properties from instrumented indentation: Uncertainties due to tip-shape correction. *J. Mater. Res*. 1998; 13(10):2936-2944.
5. Herrmann K, Jennett N, Wegener W, Meneve J, Hasche K, Seemann R. Progress in determination of the area function of indenters used for nanoindentation. *Thin Solid Films*. 2000; (377-378):394-400.
6. Sawa T, Tanaka K. Simplified method for analyzing nanoindentation data and evaluating performance of nanoindentation instruments. *J. Mater. Res*. 2001; 16(11):3084-3096.
7. Antunes J, Cavaleiro A, Menezes L, Simões M, Fernandes J, Ultra-microhardness testing procedure with vickers indenter. *Surf. Coat. Technol*. 2002; 149(1):27-35.
8. Franco ARJ, Pintaúde G, Sinatora A, Pinedo CE, Tschiptschin AP. The use of vickers indenter in depth sensing indentation for measuring elastic modulus and vickers hardness. *Mater. Res*. 2004; 7(3):483-491.
9. VanLandingham MR. Review of instrumented indentation. *J. Res. Natl. Inst. Stand. Technol*. 2003; 108(4):249-265.
10. Suganuma M, Swain MV. Simple method and critical comparison of frame compliance and indenter area function for nanoindentation. *J. Mater. Res*. 2004; 19(12):3490-3502.
11. Oliver WC, Pharr GM,. Measurement of hardness and elastic modulus by instrumented indentation: Advances in understanding and refinements to methodology. *J. Mater. Res*. 2004; 19(1):3-20.
12. Hay JL, Pharr GM. Instrumented indentation testing, In: *ASM Handbook* Volume 8, Mechanical Testing and Evaluation, 10 ed., 2000, p. 232-243. Materials Park, OH.
13. McElhaney K, Vlassak J, Nix W. Determination of indenter tip geometry and indentation contact area for depth-sensing indentation experiments, *J. Mater. Res*. 1998; 13(5):1300-1306.
14. Pharr GM, Oliver WC, Brotzen FR. On the generality of the relationship between contact stiffness, contact area, and elastic modulus during indentation. *J. Mater. Res*. 1992; 7(3):613-617.
15. Troyon M, Huang L. Correction factor for contact area in nanoindentation measurements. *J. Mater. Res*. 20(3):610-617.
16. Troyon M, Huang L. Critical examination of the two-slope method in nanoindentation. *J. Mater. Res*. 2005; 20(8):2194-2198.
17. Baker SP, Nix WD. Mechanical properties of compositionally modulated au-ni thin films: Nanoindentation and microcantilever deflection experiments, *J. Mater. Res*. 1994; 9(12):3131-3144.
18. Bolshakov A, Pharr GM. Influences of pile-up on the measurement of mechanical properties by load and depth sensing indentation techniques, *J. Mater. Res*. 1998; 13(4):1049-1058.
19. Li Z, Cheng YT, Yang HT. S. Chandrasekar, On two indentation hardness definitions. *Surf. Coat. Technol*. 2002; 154(2-3):124-130.
20. Kese KO, Li ZC, Bergaman B. Method to account for true contact area in soda-lime glass during nanoindentation with berkovich tip. *Mater. Sci. Eng*. 2005; A 404(1-2):1-8.
21. Miyahara K, Nagashima N, Matsuoka S. Development and application of a combined atomic force microscopy-nanoindentation system with a silicon tip and a diamond. *Philos. Mag*. 2002; A 82(10):2419-2160.
22. Joslin D, Oliver W. New method for analyzing data from continuos depth-sensingmicroindentation tests. *J. Mater. Res*. 1990; 5(1):123-126.
23. Stone DS, Yoder KB, Sproul WD. Hardness and elastic modulus of tin based on continous indentation technique and new correlation. *J. Vac. Sci. Technol*. 1991; 19(4):2543-2447.
24. Gong J, Miao H, Peng Z. On the contact area for nanoindentation tests with berkovich indenter: case study on soda-lime glass. *Mater. Lett*. 2004; 58(7-8):1349-1353.
25. Fischer-Crips AC. *Nanoindentation*. 1 ed. New York: Springer; 2002.
26. Meza JM, Franco EE, Buiochi F, Farias CM, Souza RM et al. *Using the ultrasound and instrumented indentation techniques to measure the elastic modulus of engineering materials*. to appear in Rev. Metal. Mad., 2007.
27. Weiler W. Dynamic loading. a new microhardness test method. *J. Test. Eval*. 1990; 18(4)229-239.
28. Simões M, Fernandes J, Cavaleiro A. The influence of experimental parameters on hardness and young's modulus determination using depth-sensing testing, *Phil. Mag*. 2002; A 82(10):1911-1919.
29. Bouzakis KD, Michailidis N, Hadjiyiannis S, Skordaris G, Erkens G. The effect of specimen roughness and indenter tip geometry on the determination accuracy of thin hard coatings stress-strain laws by nanoindentation. *Mater. Char*. 2002; 49(2):149-156.
30. Cheng YT, Cheng CM. Scaling, dimensional analysis, and indentation measurements. *Mater. Sci. Eng*. 2004; R 44:91-149.
31. Cheng YT, Cheng CM. Further analysis of indentation loading curves: Effects of tip rounding on mechanical property measurements. *J. Mater. Res*. 1998; 13(4):1059-1064.
32. Meza JM, Cruz J. *Tip bluntness effect in mechanical properties measured through nanoindentation test*. Presented at IV International congress of materials, Pereira, and in Scientia et technica. 2007; 36:613-618.
33. Meza JM, Abbes F, Troyon M. *Penetration depth and tip radius dependence on the correction factor in nanoindentation measurements*. In print in J. Mater. Res.